Electric fields yield chaos in microflows

Jonathan D. Posner[a,b], Carlos L. Pérez[c], and Juan G. Santiago[d,1]

[a]Department of Mechanical Engineering, University of Washington, Seattle, WA 98195; [b]Department of Chemical Engineering, University of Washington, Seattle, WA 98195; [c]Department of Mechanical Engineering, Arizona State University, Tempe, AZ 85287; and [d]Department of Mechanical Engineering, Stanford University, Stanford, CA 94305

Edited by* Parviz Moin, Stanford University, Stanford, CA, and approved July 30, 2012 (received for review April 23, 2012)

We present an investigation of chaotic dynamics of a low Reynolds number electrokinetic flow. Electrokinetic flows arise due to couplings of electric fields and electric double layers. In these flows, applied (steady) electric fields can couple with ionic conductivity gradients outside electric double layers to produce flow instabilities. The threshold of these instabilities is controlled by an electric Rayleigh number, Ra_e. As Ra_e increases monotonically, we show here flow dynamics can transition from steady state to a time-dependent periodic state and then to an aperiodic, chaotic state. Interestingly, further monotonic increase of Ra_e shows a transition back to a well-ordered state, followed by a second transition to a chaotic state. Temporal power spectra and time-delay phase maps of low dimensional attractors graphically depict the sequence between periodic and chaotic states. To our knowledge, this is a unique report of a low Reynolds number flow with such a sequence of periodic-to-aperiodic transitions. Also unique is a report of strange attractors triggered and sustained through electric fluid body forces.

fluid mechanics | electrohydrodynamics | electrokinetic instability

Chaos in scalar fields driven by deterministic, low Reynolds number (Re) flows was first described by H. Aref in the early 1980s (1); and chaotic advection was first leveraged to achieve fast mixing in microchannel flows by Liu et al. (2). Indeed, deterministic chaos has been studied in a wide variety of experimental systems including turbulent flows (3), chemical reactions (4), biological systems (4), and atomic force microscopy (5). Here, we report evidence demonstrating the existence of dynamic transitions from periodicity to aperiodicity and chaos in low Re electrokinetic micron-scale flows. Microfluidic devices often use liquid-phase electrokinetic phenomena to transport, concentrate, and separate samples (6). Electrokinetics is the branch of electrohydrodynamics that describes the coupling of ion transport, liquid flow, and electric fields, and it is characterized by the importance of electric double layers (7).

Typical electrokinetic flows, in order of 10 micron channels, have low Reynolds numbers and are often stable as inertial forces are strongly damped by viscous forces. However, applied electric fields can couple with heterogeneous electric properties, in particular gradients of ionic conductivity, to generate electric body forces in the bulk liquid (outside electric double layers). These body forces can drive instability of bulk liquid flow fields. This phenomena was first reported by Oddy et al. and termed electrokinetic instabilities (EKIs, see ref. 8). These electrokinetic flow instabilities are driven by electric body forces, $\rho_e \boldsymbol{E}$ (where ρ_e is the net free charge density and $\boldsymbol{E}$ is the electric field vector), in these heterogeneous regions (8, 9). These body forces can be distributed over relatively large flow regions and can exist outside of electric double layers (10, 11).

In this paper, we present compelling evidence that an unstable, low Reynolds number electrokinetic flow can become chaotic in regimes characterized by the relative importance of electrical and viscous forces. Temporal power spectra and time-delay phase-maps distinguish between periodic and chaotic regimes. We believe this is the first demonstration of a strange attractor triggered and sustained through electric fluid body forces in a low Reynolds number flow. We show that the flow exhibits at least two periodic-to-aperiodic (chaotic) transitions as the electric Rayleigh number control parameter is monotonically increased. Although such transitions are well known in the nonlinear dynamics field (12–15) and occur in Taylor-Couette flows (16) (where fluid inertia is important), we know of no reported microflow system with such a sequence of transitions.

Results and Discussion

Fig. 1 shows experimental scalar imaging of our electrokinetic flow at various (constant) values of electric field. The Reynolds numbers of these flows range from about 0.01 to 0.1 (based on hydraulic channel diameter and electroosmotic velocity). Fig. 1*A* shows a representative measured scalar concentration field of the stable base state flow in a cross shaped microchannel. Electroosmotic flow drives high-conductivity electrolyte dyed with an electrically neutral fluorescent molecule from the west (left) channel and lower conductivity background electrolyte from the north (top) and south (bottom) channels toward a common outlet in the east (right) channel. The north and south sheath streams focus the center, dyed stream into a wedge-shaped "head" structure. Downstream of the intersection ($x/w > 1$), the sheath and center streams form two diffuse conductivity interfaces, which develop within the east channel. Posner and Santiago (17) proposed that the relative strength of electric and viscous forces are described by a local electric Rayleigh number, Ra_e, of the form,

$$Ra_e = \frac{\varepsilon E_a^2 d^2}{D\mu}\frac{\gamma - 1}{\gamma}\nabla^*\sigma^*\Big|_{\max}, \qquad [1]$$

where ε is the fluid permittivity, E_a is the nominally applied and constant electric field (voltage difference between south and east channels per axial length of south and east channels), d is the channel depth, D is the effective diffusivity of the ions, and μ is the fluid viscosity. $\nabla^*\sigma^*|_{\max}$ is a nondimensional maximum transverse conductivity gradient in the flow (see ref. 17). For our flows, a critical electric Rayleigh number of about 200 results in an easily observable EK flow instability (17).

Below a critical Rayleigh number of about $Ra_{e,l}^{\text{crit}} = 200$, the flow is stable (c.f. Fig. 1*A*). For $Ra_e > 205$, a sinuous dye pattern develops and disperses as it advects downstream, as shown in Fig. 1*B*. A further increase of the Rayleigh number of less than 2% results in disturbances that grow (briefly) exponentially in space and roll up in alternating sequences, qualitatively similar in appearance to Bénard-von Kàrmàn vortex street (18, 19 and see Fig. 1 *C* and *D*). At Ra_e values of 326 and 437, the scalar fields are highly asymmetric about the channel axial centerline, as shown in Fig. 1 *E* and *F*. In these highly unstable conditions, the wedge-shaped head aperiodically oscillates strongly along the spanwise direction. This strongly unstable flow results in highly disordered

Author contributions: J.D.P. and J.G.S. designed research; J.D.P. performed experiments; J.D.P., C.L.P., and J.G.S. analyzed data; and J.D.P., C.L.P., and J.G.S. wrote the paper.

The authors declare no conflict of interest.

*This Direct Submission article had a prearranged editor.

[1]To whom correspondence should be addressed. E-mail: juan.santiago@stanford.edu.

This article contains supporting information online at www.pnas.org/lookup/suppl/doi:10.1073/pnas.1204920109/-/DCSupplemental.

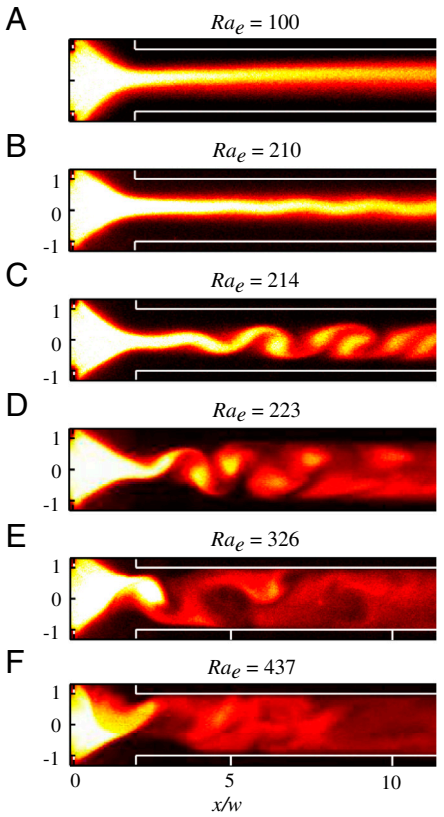

Fig. 1. Representative instantaneous scalar concentration fields of unstable electrokinetic flows, each subject to constant electric field. The center-to-sheath conductivity ratio γ is 100 and the electric Rayleigh number Ra_e is indicated above each image. For our parameters, the conversion between electric field and Rayleigh number is $E = 1.78Ra_e$ for electric field in V/cm.

scalar patterns and a well-mixed fluid a few channel widths downstream.

Fig. 2*A* shows a map of the temporal spectral intensity as a function of the electric Rayleigh number (abscissa) and temporal frequency (ordinate). Spectral density was calculated using a normalized fluorescence intensity of the form,

$$I'(t) = \frac{(I(t) - \langle I \rangle_t)}{\langle I \rangle_t}, \qquad [2]$$

where $I'(t)$ is the fluorescence intensity taken at a point on the channel centerline and $x/w = 2$ and the angle brackets and subscript t denote a temporal average. For Ra_e less than about 200, the flow is stable and the power spectrum only shows power near DC and low-amplitude image noise. Starting near $Ra_e = 205$, we observe periodic motion with at fundamental frequency of $f_1 = 42$ Hz (at $Ra_e = 205$) and weak harmonics at $2f_1$ and $3f_1$, consistent with the periodic dye pattern of Fig. 1*B*. In the range $230 < Ra_e < 325$, the frequency of the fundamental and harmonic peaks slowly decrease, which coincides with an increase in the disturbance wavelength, perhaps due to increasing electroosmotic flow (17). Subharmonic intensity peaks associated with period doubling bifurcations are evident in the region near $Ra_e = 290$–350 (20). As an example, we labeled the subharmonic peak at $f_1/2$, but we also observe peaks at $3f_1/4$ and $5f_1/6$. As we discuss below, further increases in Ra_e result in a transition to fully chaotic, aperiodic behavior. Such transitions from steady state to time-dependent solutions, then period doubling, and eventually fully chaotic behavior are well known in fluid flows. However, it is most common for complexity in these flows to increase monotonically with an increase of the controlling para-

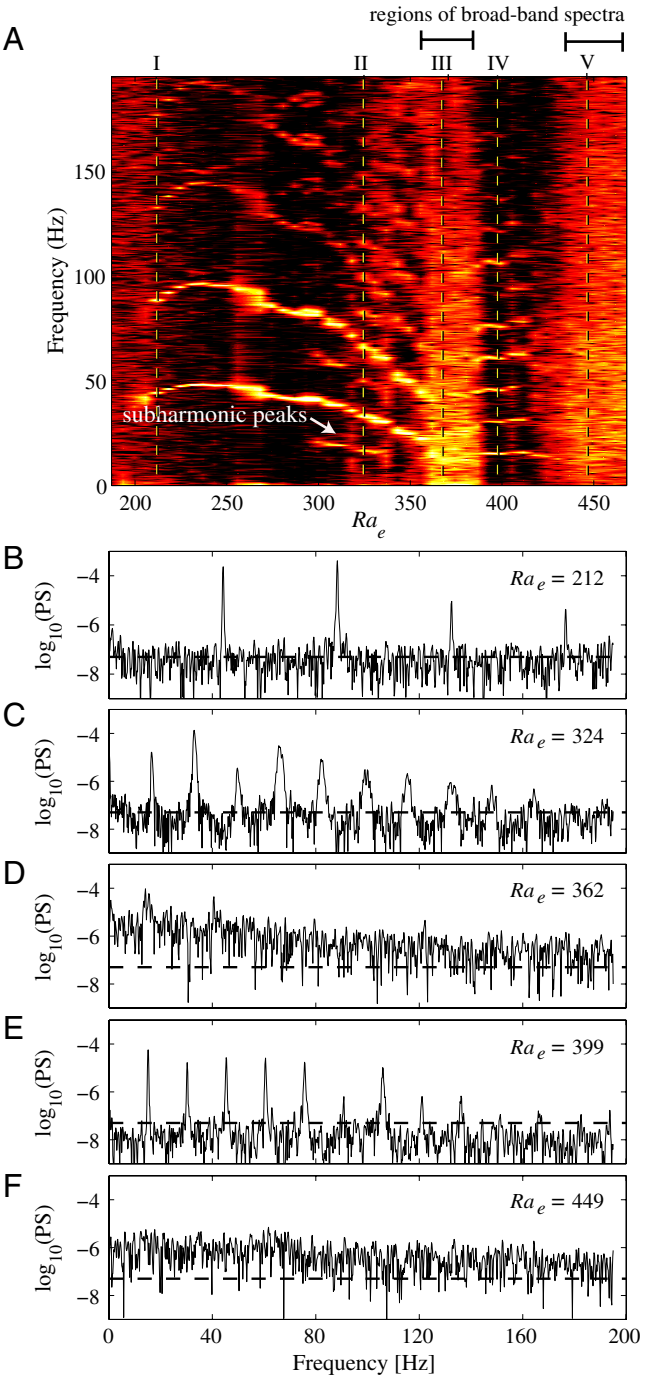

Fig. 2. (*A*) Temporal power spectrum of $I'(t)$ (in $\log_{10}$) as a function of electric Rayleigh number and temporal frequency, f. Black and white colors represent low and high spectral intensity, respectively. For $Ra_e < 200$, the flow is stable (energy concentrated near $f = 0$). Spectrum contains a fundamental frequency and harmonics for $205 < Ra_e < 325$. Subharmonic peaks appear at $Ra_e = 290$–350. Aperiodic regimes are observed for Ra_e ranges of 350–390 and 415–490 (labeled with horizontal bands above figure). Aperiodic regimes are defined here as those exhibiting a broadband power spectrum that is at least one order of magnitude above instrument noise. The individual power spectra at five representative Ra_e are shown in (*B*–*F*) and denoted with a roman numeral and vertical dashed line in (*A*). (*B*) Power spectrum (in semilog coordinates) for $Ra_e = 212$ shows flow instability with a single-fundamental frequency at $f = 42$ Hz and harmonics $2f$ and $3f$. (*C*) Spectrum for $Ra_e = 324$ shows subharmonic peaks. (*D*) Aperiodicity with broadband spectrum above instrumental noise (dashed line). (*E*) Second time-periodic state with at least 11 observable harmonics. (*F*) Final chaotic state.

meter. For example, increasing Rayleigh number, Ra, in Rayleigh-Bernard flows (13) results in transitions from steady flow to time-dependent flow and, eventually, to fully chaotic, aperiodic behavior.

The most interesting aspect of the current flow is the fact that, unlike classic low-Reynolds fluid flows, the relation between the controlling parameter, Ra_e, and dynamic complexity of the system is not monotonic. As we increase Ra_e we observe steady behavior ($Ra_e < \sim 200$) and this is followed by time-periodic dynamics including a series of four harmonics ($Ra_e = 200$ to 290), evidence of period doubling ($Ra_e = 290$ to 350), transition to a chaotic state (350 to 390), a second time-periodic state with at least 11 observable harmonics (390 to 415), and then a second, final chaotic state ($Ra_e > 415$ to 490). That is to say, surprisingly, the flow transitions sequentially in and out of chaos as Ra_e increases so that, as the electric Rayleigh number is increased from 200 to 490, we observe two sequential aperiodic regimes, each of which is preceded by time-periodic regimes.

The two aperiodic regimes are labeled as solid horizontal bands above Fig. 2*A*. The regimes at $Ra_e \sim 350$–390 and $Ra_e > 415$ are strongly aperiodic as evidenced by well-distributed spectral content (greater than 1 order of magnitude above noise, as shown in Fig. 2 *B*–*F*). Other regions show some evidence of aperiodicity, such as the region near $Ra_e \sim 320$–340, which has some broadband spectral content, but not as strongly as the latter two regimes. Note that although the distinction between periodic and aperiodic dynamics is typically made based on the existence of broadband spectra, the minimum strength of broadband spectra that warrants identification as aperiodicity is arbitrary. Broadband spectra values significantly above 1 order of magnitude above instrument noise leaves us reasonably confident that aperiodic dynamics exist. This definition is supported by the phase maps presented below. The first and second aperiodic regimes are also separated by a periodic region ($Ra_e \sim 390$–415) with a fundamental of $f_2 = 15.8$ Hz and harmonics at $2f_2, 3f_2 \ldots 11f_2$ (see dashed line IV at $Ra_e = 399$ in Fig. 2*A*). Periodic windows sandwiched between aperiodic regimes have been observed experimentally in, for example, the Belousov-Zabotinsky reaction (21) and in moderately high Reynolds number Taylor-Couette flow (3, 16, 22). They are also well known as in mathematical models with one-dimensional mappings such as the Rössler attractor (4). To our knowledge, the current paper is the first reported instance of a sequence of alternating periodic-chaotic dynamical states in a low-Reynolds number flow system. In this microflow, monotonic increase of the Ra_e controlling parameter (proportional to electric field) drives the flow sequentially into and out of chaos.

Example power spectra of the periodic and aperiodic regimes are shown in Fig. 2 *B*–*F* for $Ra_e = 212$, 324, 362, 399, and 449, respectively. These Ra_e values are highlighted in Fig. 2*A* using vertical dashed lines labeled I to V. At $Ra_e = 212$, we see distinct sharp peaks in the power spectra at the fundamental frequency $f_1 = 42$ Hz and at harmonics $2f_1$, and $3f_1$. At $Ra_e = 324$, we observe clear evidence of period doubling and a broadening of peaks as frequency increases. In the first chaotic region, at $Ra_e = 362$, we observe broadband spectral content tapering off at higher frequencies and well above background noise. At $Ra_e = 399$, we observe the second periodic region, including a series of over 11 harmonics. Lastly, at $Ra_e = 449$, we observe the second chaotic regime, which persists until the high-field limitations of our experimental setup.

We constructed multidimensional phase-maps from time series of normalized fluorescent intensity values, $I'(t_k)$ $(k = 1 \ldots 2{,}000)$, taken at $x/w = 2$ and $y/w = 0$ using the method of time delays (23, 24). Here, time delay τ is used to construct a sequence of m-dimensional points $[I'(t_k), I'(t_k + \tau), \ldots I'(t_k + \tau(m-1)]$ resulting in an m-dimensional phase-space trajectory. We employed the method of Fraser and Swinney to obtain an optimum τ defined by the first minimum of the mutual information function (25). Fig. 3 shows $I'(t + \tau)$ versus $I'(\tau)$ phase-maps for $Ra_e = (a)212$, (b) 324, (c) 362, (d) 399, and (e) 449 for $\tau = 2.6$ ms. The sequence

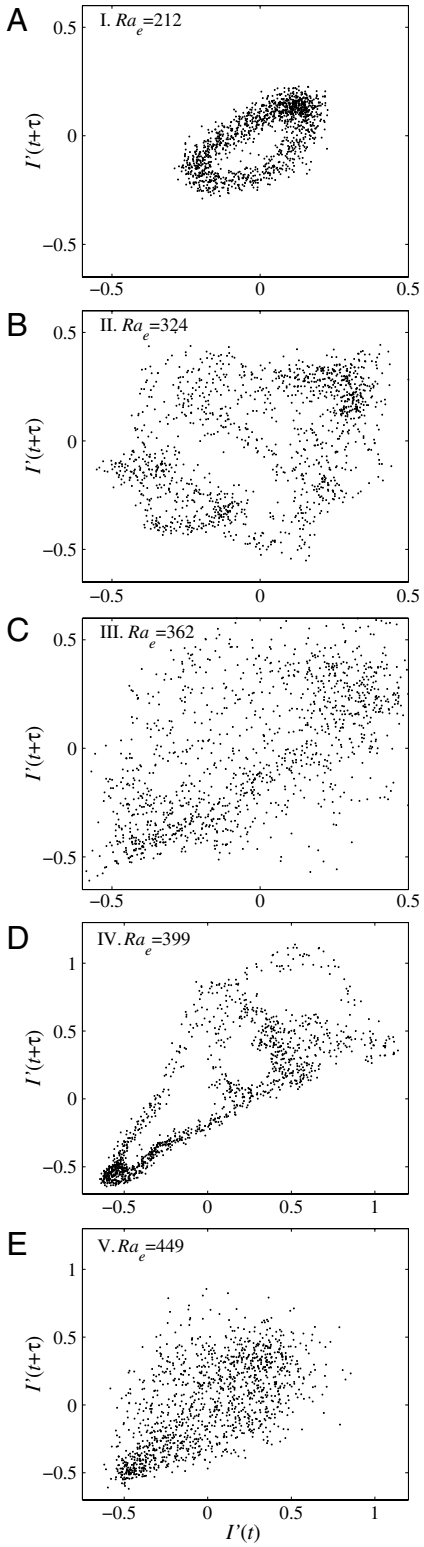

Fig. 3. Phase-maps ($I'(\tau)$, $I'(t + \tau)$) for $Ra_e = (A)212$, (*B*) 324, (*C*) 362, (*D*) 399, and (*E*) 449. Together they illustrate the alternating sequence of periodic-chaotic dynamical behavior that occurs as Ra_e is swept from 190 to 490. The axis limits for *D* and *E* are expanded for clarity. The power spectra contours (in the Ra_e vs. frequency plane) for each Ra_e number case shown here is labeled with a roman numeral in Fig. 2*A*.

of attractors illustrates the sequence of periodic to aperiodic dynamics transitions observed in the range of Ra_e of 150–490 with each map showing between 50–120 orbits. For $Ra_e = 212$ (Fig. 3*A*) the attractor shows an elliptical geometry (with a curve thickness, which we attribute to experimental image noise) characteristic of periodic dynamics. Well into the first periodic regime and in the period doubling region, at $Ra_e = 324$, the attractor is multidimensional, as shown in Fig. 3*C*. Here, more complex temporal evolution is characterized by weaving of smaller orbits within larger ones. At $Ra_e = 362$, we are within the aperiodic power spectrum of the first chaotic regime (see Fig. 2 *A* and *D*), and the respective attractor (cf. Fig. 3*C*) shows a dramatic change including significant spreading of the orbits throughout the phase map. Spreading of attractor orbits of chaotic flow has been observed experimentally in the multiple periodic-to-chaotic regime transitions in Taylor-Couette flows (3, 22). The phenomenon is also evident in classical dynamical systems attractors such as the Rössler attractor and the differential-delay equation (Mackey-Glass (4). Fig. 3*D* ($Ra_e = 399$) shows the transition back to a more ordered, periodic state as Ra_e is increased, and the attractor shows a much tighter set of orbits. Fig. 3*E* shows the dynamical structure for $Ra_e = 449$ within the second aperiodic regime. Here, the geometric structure found in previous attractors is lost, suggesting higher attractor dimensionality and dynamics reminiscent of turbulence, but occurring here at Reynolds numbers less than about 0.1.

The power spectra and phase-maps collectively are strong evidence that the regions of aperiodicity are chaotic. Our data show compellingly that that low Reynolds number EKI flows exhibit alternating regimes of periodic motion and low dimensional chaos. The transitions between periodic and aperiodic dynamics occur twice (within Ra_e ranges of 350–390 and $Ra_e > 415$) as the electric Rayleigh number is monotonically varied from 190 to 490. To our knowledge, this is the first report of such a sequence of order-chaos transitions in low Reynolds number flows.

Materials and Methods

The experiments reported here were performed at the Stanford Microfluidics Laboratory in Stanford University. We performed experiments in glass, cross-shaped microchannels isotropically etched (D-shape) to $w = 50$ μm wide and 20 μm deep (Micralyne, Alberta, Canada). Direct current (DC) electrical potentials and current were applied by submerging platinum wire electrodes in the electrolyte solutions at end-channel reservoirs. We obtained instantaneous concentration fields of rhodamine B dye using epifluorescence microscopy, high speed CCD camera imaging (Roper Scientific, Tucson, Arizona). This dye is electrically net neutral (26) with a molecular weight of 479 g/mol; so our images are those of a passive, diffuse scalar and motion perpendicular to material lines is due to advection of the bulk solvent (water) and not a drift velocity due to the electric field. Potentials and CCD image acquisitions were synchronized using a high voltage sequencer (LabSmith, Livermore, CA, USA). Flows were imaged with a microscope (Nikon, Japan) equipped with a 20X, NA = 0.45 ELWD objective (Nikon, Japan). More details of the experimental setup and conditions are given by Posner and Santiago (17) additional details on the image acquisition and data analysis can be found in the *SI Text*.

ACKNOWLEDGMENTS. This work was supported by NSF PECASE (J.G.S. award number CTS-0239080 and CAREER (J.D.P. award number CBET-0747917) Awards.

1. Aref H (1984) Stirring by chaotic advection. *J Fluid Mech* 143:1–21.
2. Liu RH, et al. (2000) Passive mixing in a three-dimensional serpentine microchannel. *J Microelectromech Syst* 2:190–197.
3. Brandstäter A, Swinney HL (1987) Strange attractors in weakly turbulent Couette-Taylor flow. *Phys Rev A* 35:2207–2220.
4. Olsen LF, Degn H (1985) Chaos in biological systems. *Q Rev Biophys* 18:165–225.
5. Hu S, Raman A (2006) Chaos in atomic force microscopy. *Phys Rev Lett* 96:036107.
6. Squires TM, Quake SR (2005) Microfluidics: Fluid physics at the nanoliter scale. *Rev Mod Phys* 77:977–1026.
7. Saville DA (1997) Electrohydrodynamics: The Taylor-Melcher leaky dielectric model. *Annu Rev Fluid Mech* 29:27–64.
8. Oddy MH, Santiago JG, Mikkelsen JC (2001) Electrokinetic instability micromixing. *Anal Chem* 73:5822–5832.
9. Lin H (2009) Electrokinetic instability in microchannel flows: A review. *Mech Res Commun* 36:33–38.
10. Melcher JR, Taylor GI (1969) Electrohydrodynamics: A review of the role of interfacial shear stresses. *Annu Rev Fluid Mech* 1:111–146.
11. Hoburg JF, Melcher JR (1979) Internal electrohydrodynamic instability and mixing of fluids with orthogonal field and conductivity gradients. *J Fluid Mech* 73:333–351.
12. Feigenbaum MJ (1983) Universal behavior in nonlinear systems. *Physica D* 7:16–39.
13. Giglio M, Musazzi S, Perini U (1981) Transition to chaotic behavior via a reproducible sequence of period-doubling bifurcations. *Phys Rev Lett* 47:243–246.
14. Lauterborn W, Cramer E (1981) Subharmonic route to chaos observed in acoustics. *Phys Rev Lett* 47:1445–1448.
15. Simoyi RH, Wolf A, Swinney HL (1982) One-dimensional dynamics in a multicomponent chemical reaction. *Phys Rev Lett* 49:245–248.
16. Buzug T, von Stamm J, Pfister G (1993) Characterization of period-doubling scenarios in Taylor-Couette flow. *Phys Rev E* 47:1054–1065.
17. Posner JD, Santiago JG (2006) Convective instability of electrokinetic flows in a cross-shaped microchannel. *J Fluid Mech* 555:1–42.
18. Bénard H (1908) Formation des centres de gyration à l'arrière d'un obstacle en mouvement. *C R Acad Sci Paris* 147:839–842.
19. von Kármán T, Rubach H (1912) Über den mechanismus des flüssigkeits- und luftwiderstandes. *Phys Z* 13:49–59.
20. Moon FC (1992) *Chaotic and Fractal Dynamics* (Wiley, New York).
21. Turner JS, Roux J-C, McCormick WD, Swinney HL (1981) Alternating periodic and chaotic regimes in a chemical reaction—Experiment and theory. *Phys Lett A* 85:9–12.
22. Brandstäter A, et al. (1983) Low-dimensional chaos in a hydrodynamic system. *Phys Rev Lett* 51:1442–1445.
23. Packard NH, Crutchfield JP, Farmer JD, Shaw RS (1980) Geometry from a time series. *Phys Rev Lett* 45:712–716.
24. Takens F (1981) *Dynamical Systems and Turbulence* (Springer, Berlin).
25. Fraser AM, Swinney HL (1986) Independent coordinates for strange attractors from mutual information. *Phys Rev A* 33:1134–1140.
26. Schrum KF, Lancaster JM, III, Johnston SE, Gilman SD (2000) Monitoring electroosmotic flow by periodic photobleaching of a dilute, neutral fluorphore. *Anal Chem* 72:4317–4312.

Supporting Information

Posner et al. 10.1073/pnas.1204920109

SI Text

Data Acquisition and Analysis. ***Summary of data acquisition and instances of data rejection.*** We here summarize some features of our scalar image data acquisition. Further details can be found in ref. 1. The quantitative scalar field data we present in Figs. 2 and 3 are based on image sequences of 45 experiments comprising 45 applied electric fields (nominal electric fields from 333 to 1122 V/cm). These imaging experiments were strictly limited by trade-offs between camera sensitivity, frame rate, region of interest analyzed (subset of pixels used in CCD), and the amount of data that fit in the RAM of our data acquisition computer. We used a 16-bit, Peltier-cooled Photometrics CCD with on-chip gain (Tucson, AZ). We chose a frame rate of 390 Hz. The data sets each consisted of 1620 16-bit images with a CCD region of interest of only 3×512 pixels (to reduce required memory and increase data rate). One exception to this is the data of the lowest electric field (a stable case) for which we obtained only about 1000 images (and extended these data to match the duration of the other image series). The data of about half of the 12th electric field and all of the 13th electric field (at $E = 455$ and 466 V/cm) were likely corrupted by severe background illumination (we attribute this to unshielded lighting from the room). We therefore replaced the last approximately one-third of data record 12 with a copy of its first approximate one-third, and replaced all of the data record 13 with the new data record 12. In all, we replaced <3% of the data (about 1.3 of the 45 records) shown in Fig. 2.

Further details of power spectrum analysis. We performed the KPSS Test (2) to assess the stationarity of each of the experiments shown in Fig. 2. We used the kpsstest function in Matlab (Mathworks) and used parameters recommended by Kwiatkowski et al (2), including a 95% significance (alpha = 0.05) level. In 40 of the 45 experiments, the test showed a failure to reject the null hypothesis that the time series was trend stationary; suggesting the data were trend stationary. Four of the remaining data sets were spread apparently randomly in the low-electric field periodic regimes (at the 3rd, 14th, 16th, and 25th lowest Ra_e cases shown in Fig. 2). We attribute this to some slight fluctuation of the illumination intensity supplied by our microscope's mercury bulb. The remaining, single data series, which was suggested by the test to be nonstationary occurred within the first chaotic region in Fig. 2. However, the KPSS Test suggested the other six experiments in this same chaotic region were stationary.

Prior to performing the power spectra, we removed slight linear trends. These linear trends are common in fluorescence quantitation of electrokinetic microflows and attributable to various effects including variations in light intensity of the illumination (in our case, the mercury bulb of the microscope), effects of electrochemical reactions (at end channel reservoirs containing electrodes) on the tracer dye, and/or photobleaching of the dye. The typical linear trend in the data consisted of a variation of less than about $\pm 3\%$ of the measured mean value. The linear trend in 42 of 45 cases varied less than $\pm 7\%$ and all varied less than $\pm 11\%$.

Prior to computing power spectra on the data, we used a symmetric Hann window to minimize frequency leakage. Fig. 2 presents a map of 45 power spectra of the windowed time series up to the Nyquist folding frequency of 195 Hz.

Lastly, the data shown in Fig. 2 used a virtual point detector centered at $x/w = 2$. We integrated the intensity in a 3×3 region in this subimage as a virtual point detector for our power spectra. We also analyzed power spectra for temporal fluctuations of the scalar at following additional downstream locations: $x/w = 3.5$, 5.3, and 7.1. These power spectra maps were qualitatively very similar to those near $x/w = 2$, except for an expected attenuation of the high frequency power due to the dispersion associated with the combined effects of advection and molecular diffusion. This similarity included the harmonics of the first (low electric field) periodic regime, evidence of period doubling, the clear delination of two chaotic regions, and the harmonics of the second (high electric field) periodic regime.

1. Posner JD, Santiago JG (2006) Convective instability of electrokinetic flows in a cross-shaped microchannel. *J Fluid Mech* 555:1–42.

2. Kwiatkowski D, Phillips PCB, Schmidt P, Shin Y (1992) Testing the null hypothesis of stationarity against the alternative of a unit root. *J Ecol* 54:159–178.